

Resilient AFE Drive Control using Neural Networks with Tracking Guarantees[★]

Nicolas Kirsch^{*} Catalin Arghir^{**} Silvia Mastellone^{**}
Giancarlo Ferrari-Trecate^{*}

^{*} *École Polytechnique Fédérale de Lausanne, DECODE lab, Lausanne, Switzerland (e-mail:{nicolas.kirsch, giancarlo.ferraritrecate}@epfl.ch)*

^{**} *FHNW University of Applied Sciences and Arts Northwestern Switzerland, Windisch, Switzerland (email:silvia.mastellone@fhnw.ch, carghir@ethz.ch)*

Abstract: Industrial installations across several sectors have seen a dramatic increase in productivity, accuracy and efficiency over the last decade due to expanded utilization of medium voltage, variable speed power electronic converters to drive their processes. Specifically, active front-end (AFE) drives have become popular due to their ability to deliver power while maintaining safe electrical setpoints. However, under abnormal grid conditions such as phase loss, conventional AFE control may fail to enforce safety constraints, potentially leading to drive shutdown and significant financial losses.

In this work, we propose using reference-tracking Performance Boosting (rPB) to improve the resilience of standard AFE control to faults. This neural-network control framework provides a principled way to optimize transient performance while preserving the steady-state tracking properties of AFE-based drives. By carefully shaping the input signals to the rPB controller, we ensure that it activates only during grid faults, leaving nominal operation unaffected. Simulation results show that the proposed approach successfully maintains the DC bus voltage and the grid current within safe limits during single-phase loss events.

Keywords: Nonlinear optimal control, Neural Network Control, Active Front End Drives, Fault Ride-Through

1. INTRODUCTION

Modern power grids are increasingly adopting active front-end (AFE) converters serving not only in interfacing renewable generation, such as wind and hydro, but also in flexible industrial loads including large compressors, heat pumps, and pumped-hydro drives (Hokayem et al., 2024). These systems may require bidirectional power flow, operating alternately as energy consumers and sources, and thus form the cornerstone of a new class of grid-interactive electrical assets. Apart from handling the AC current and regulating the DC bus, AFEs may enable ancillary services such as reactive power compensation and inertia emulation, even in traditional motor drive applications (Arghir et al., 2025).

These functions are typically implemented through a standard cascaded PI-based control architecture, including an inner loop for current regulation, and an outer DC-bus voltage controller, delivering high performance under nominal grid conditions. However, perturbed grid states such as voltage sags, asymmetrical faults, or weak-grid operation significantly degrade converter performance (Baeckeland et al., 2024; He et al., 2024; Stanojev et al., 2025). Un-

der these disturbances, the AFE struggles to keep its controlled variables within constraints, particularly the DC-bus voltage, which may experience severe under-voltage. Such deviations frequently trigger protective shutdowns, interrupting industrial processes and leading to significant productivity losses (Hosseinzadehtaher et al., 2024; Eslahi et al., 2023). Typical fault ride-through strategies rely on modifying the current reference, either through dynamic limiters (Tang et al., 2025) or mode-switching logic that adapt the reference upon fault detection (Bottrell and Green, 2014). While effective, limiter-based approaches can lead to current distortion during asymmetrical faults, and mode-switching methods are usually limited to short-circuit or deep-sag events (Zarei et al., 2019). Maintaining both continuous operation and safe, bounded dynamics during large electrical disturbances remains an open issue in modern AFE-equipped drives (Wang et al., 2025).

Within the broader theory of reference tracking for nonlinear systems, several approaches have been considered to improve transient performance. Model Predictive Control (MPC) approaches can track time-varying references while incorporating secondary, potentially nonlinear objectives through constraints or the loss function (Ferramosca et al., 2009), sometimes with closed loop guarantees (Limon et al., 2018). However, the deployment of MPC policies typically requires solving complex optimization problems in real time. This can be computationally impractical when

[★] This research has been supported by the Swiss National Science Foundation under the NCCR Automation (grant agreement 51NF40.180545) and the NECON project (grant number 200021-219431).

dealing with highly non-linear models and cost functions (Rawlings et al., 2017).

In adaptive control, the controller is adjusted in real-time based on the system's performance (Nguyen, 2018), and constraint satisfaction is typically enforced using barrier functions (Kong et al., 2023) or safety filters (Schneeberger et al., 2024). While these methods are promising, closed-loop guarantees are usually restricted to stability and constraint satisfaction and often apply locally.

Neural networks have also been studied to improve reference tracking, but mainly as observers (Park et al., 2017; Gao et al., 2019) or to optimize tracking metrics, often without providing guarantees (Zhang et al., 2022). The authors of (Kirsch et al., 2025) introduced a neural network controller with reference tracking guarantees. This neural controller works as a plug-in supporting pre-existing reference tracking controllers during transient while not interfering in steady state. Most importantly, (Kirsch et al., 2025) shows how to parametrize *all and only* reference tracking controllers in terms of a free operator satisfying mild input to output conditions. This allows improving the performance of the controller for any nonlinear objective using unconstrained optimization methods, enhancing the expressivity and reducing the computational burden. Simulation results have shown promising improvement on simple systems, making this method seemingly valuable for the support of standard active front end control during faults.

Contributions

In this paper, we apply the novel neural network-based controller architecture known as rPB to AFE drives. Our goal is to design an outer control loop that maintains stable operation even under grid faults. The rPB framework parametrizes all and only reference-tracking controllers in terms of a free operator, which enables us to optimize non-linear safety objectives in an unconstrained manner while preserving the tracking properties of the AFE controller. By carefully designing the input signals, we ensure that the rPB controller activates precisely when required, and only then, even in the presence of prolonged or sequential faults.

To demonstrate the effectiveness of the proposed approach, we test the controller on a scenario of single-phase voltage drops of varying amplitudes in the supply grid. The neural network is trained on a realistic drive simulation, and results show that the rPB controller successfully maintains system safety even in the event of a complete loss of one grid phase.

The paper is structured as follows: Section 2 describes the system and the AFE controller. Section 3 introduces the rPB control approach, formulates the converter control design problem and details the solution approach. Section 4 demonstrates the controller effectiveness in simulation based case studies and finally Section 5 contains concluding remarks and future work.

Notation

Across the paper we will be adopting the following notation: the set of all sequences $\mathbf{x} = (x_0, x_1, x_2, \dots)$, where

$x_t \in \mathbb{R}^n$, $t \in \mathbb{N}$, is denoted as ℓ^n . Moreover, \mathbf{x} belongs to $\ell_p^n \subset \ell^n$ with $p \in \mathbb{N}$ if $\|\mathbf{x}\|_p = (\sum_{t=0}^{\infty} |x_t|^p)^{\frac{1}{p}} < \infty$, where $|\cdot|$ denotes any vector norm. We say that $\mathbf{x} \in \ell^n$ if $\sup_t |x_t| < \infty$. When clear from the context, we omit the superscript n from ℓ^n and ℓ_p^n . An operator $\mathbf{A} : \ell^n \rightarrow \ell^m$ is said to be *causal* if $\mathbf{A}(\mathbf{x}) = (A_0(x_0), A_1(x_{1:0}), \dots, A_t(x_{t:0}), \dots)$, and \mathbf{A} is said to be ℓ_p -stable if it is *causal* and $\mathbf{A}(\mathbf{w}) \in \ell_p^m$ for all $\mathbf{w} \in \ell_p^n$, with $p \in \mathbb{N} \cup \{\infty\}$. Equivalently, we write $\mathbf{A} \in \mathcal{L}_p$. We say that an \mathcal{L}_p operator $\mathbf{A} : \mathbf{w} \mapsto \mathbf{u}$ has finite \mathcal{L}_p -gain $\gamma(\mathbf{A}) > 0$ if $\|\mathbf{u}\|_p \leq \gamma(\mathbf{A})\|\mathbf{w}\|_p$, for all $\mathbf{w} \in \ell_p^n$.

2. SYSTEM DESCRIPTION

We consider a medium-voltage drive system, where the AFE is implemented using a three-level active neutral-point-clamped (ANPC) converter. On the load-side, we consider a three-level ANPC converter connected to an Induction Machine (IM) model whose rotor is part of a 6MW complex driveline shaft model. The air-gap torque τ_m acts on one end of the shaft and the load τ_l on the other. The motor torque is produced through (an industry-standard) direct MPC which takes τ_m^* as reference. This setup is depicted in Fig. 1.

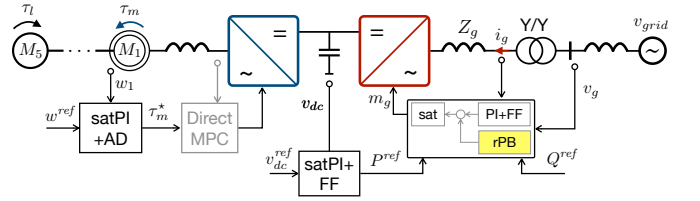


Fig. 1. Block diagram of a typical AFE-drive system with a complex driveline shaft. The control includes inner and outer loops implementing anti-windup PI compensators with active damping (AD) and feed-forward (FF) terms where appropriate. In yellow we highlight the proposed rPB control augmentation.

2.1 Drive system model

For our control design purpose, we shall omit the motor and the torque control dynamics and assume that the torque τ_m perfectly tracks the reference τ_m^* . We adopt the energy-preserving, average-switch model of the back-to-back drive system used in (Chandrasekaran et al., 2025; Arghir et al., 2025), which we discretise using forward Euler with a step time of $h = 2.5 \cdot 10^{-4} s$, yielding:

$$w_{t+1} = (1 - \frac{hD}{M})w_t + \frac{h}{M}\tau_{m,t} - \frac{h}{M}\tau_{l,t} \quad (1a)$$

$$v_{dc,t+1} = (1 - \frac{hG_{dc}}{C_{dc}})v_{dc,t} - \frac{h}{C_{dc}}\frac{\tau_{m,t}}{v_{dc,t}}w_t + \frac{h}{C_{dc}}m_{g,t}^\top i_{g,t} \quad (1b)$$

$$i_{g,t+1} = (I - hL_g^{-1}R_g)i_{g,t} + hL_g^{-1}v_{g,t} - hL_g^{-1}m_{g,t}v_{dc,t} \quad (1c)$$

where M, D are the moment of inertia and viscous damping of the driveshaft, w its angular velocity, τ_m is a control input, τ_l is a disturbance, v_{dc} is the DC-link voltage, C_{dc}

its capacitance and G_{dc} its parallel conductance. Furthermore, $m_g \in \mathbb{R}^2$ is the grid-side converter modulation vector (control input), $L_g, R_g \in \mathbb{R}^{2 \times 2}$ the phase inductance and resistance respectively, with strictly positive entries. The vector $i_g \in \mathbb{R}^2$ is the grid current (towards the converter) and $v_g \in \mathbb{R}^2$ is the voltage (measured disturbance). All two-dimensional quantities are considered to be power-invariant $\alpha\beta$ -coordinate representations of three-phase signals. Overall, (1) is a nonlinear model with states $[w, v_{dc}, i_g]$, inputs $[\tau_m, m_g]$, and disturbances $[\tau_l, v_g]$.

Given the fast response of the inner motor control loop, we assume that we can directly actuate τ_m in (1). Our motivation is based on the fact that most modern MV motor controllers adopt a form of Direct Torque Control (DTC) (Geyer et al., 2008; Tiitinen and Surandra, 1996), to track the torque set-point with high bandwidth.

We adopt the state of the art control structure described in (Chandrasekaran et al., 2025) and shown in Figure 1. An outer loop PI controller is designed to track w^{ref} through τ_m , and the two inner loop PI controllers are designed to track v_{dc}^{ref} and Q^{ref} by actuating m_g , where $Q = v_q i_d - v_d i_q \in \mathbb{R}$ is the reactive power from the grid. The reference signals are constant over the time horizon and lie within the admissible operating range of the considered drive.

3. CONTROL METHODOLOGY

The standard AFE control strategy ensures accurate tracking and constraint satisfaction under nominal operation, such as steady load torque τ_l and balanced, constant grid voltage v_g . However, when exposed to perturbed conditions, the controller may fail to maintain the DC bus voltage within its allowable operating range, potentially triggering system shutdown.

To address this, our objective is to design an auxiliary outer control loop that supports the existing controller during fault transients, ensuring constraint satisfaction without degrading nominal tracking performance. This additional layer should remain inactive during steady-state operation, thereby preserving the high-quality reference tracking of the base controller. The reference tracking performance boosting framework presented in the following section provides a suitable option to achieve this balance between fault compensation and nominal performance.

3.1 rPB Controllers

The rPB controller is a plug-in neural network controller which boosts the transient performance of a pre-existing tracking controller while preserving its guarantees in steady-state. It does so by learning to solve a Nonlinear Optimal Control problem (NOC). Its objective is not to replace controllers achieving steady-state reference tracking, but to support them during aggressive transients that might cause extreme voltage deviation in the capacitor and lead to system shutdown.

We can make the drive dynamics compatible with the rPB framework by reformulating them as follows. First, we introduce the concatenated sequence $\boldsymbol{\eta} \in \ell^8$, which collects the full closed loop states between the system and the PIs. It consists of the three system states, one of which is

two-dimensional, along with the three PI integrator states, one of which is also two-dimensional. We do the same for the references, giving $\mathbf{y}_{ref} = [w^{ref}, v_{dc}^{ref}, Q^{ref}] \in \mathbf{Y}_{ref}$, with $\mathbf{Y}_{ref} \subset \ell^3$ being the set of all references which can be tracked by the base system.

Within the rPB framework, it is assumed that the system is subject to an additive disturbance signal in ℓ_p . However, neither the load torque τ_l nor the grid voltage v_g satisfies this assumption, as neither asymptotically decays, even in the presence of faults. To address this, we decompose the grid voltage into two components: the nominal voltage \bar{v}_g and a perturbation term δv_g , such that

$$v_g = \bar{v}_g + \delta v_g.$$

During grid faults, the supplied voltage deviates from its nominal value, implying $\delta v_g \neq 0$, while otherwise $\delta v_g = 0$. Under the assumption of a finite number of faults with finite duration, the sequence $\delta \mathbf{v}_g$ belongs to ℓ_p . Since v_g enters the system linearly, we can treat $\delta \mathbf{v}_g$ (scaled by the factor hL_g^{-1}) as the required ℓ_p additive disturbance within the rPB formulation. Finally, we encode the system's initial condition within this disturbance, yielding the sequence $\mathbf{p} = (p_0, p_1, \dots, p_T) \in \ell^{10}$, where:

$$p_0 = \begin{bmatrix} \eta_0 \\ 0_{2 \times 1} \end{bmatrix}, p_t = \begin{bmatrix} 0_{8 \times 1} \\ hL_g^{-1} \delta v_{g,t} \end{bmatrix} \quad \text{for } t = 1, \dots, T,$$

where $T \in \mathbb{R}$ is the horizon. The disturbance which are not ℓ_p sequences are also concatenated, giving $\mathbf{d} = [\tau_l, \bar{v}_g] \in \mathbf{D}$, with $\mathbf{D} \subset \ell^3$ the set of acceptable nominal disturbances.

We also define $\mathbf{u} \in \ell^m$ as the control action coming from the rPB controller. There is no assumptions as to how \mathbf{u} influences the base system. Letting $f : \mathbb{R}^8 \times \mathbb{R}^m \times \mathbb{R}^3 \times \mathbb{R}^3 \rightarrow \mathbb{R}^8$ represent the closed loop dynamics of the base system with controller, we obtain:

$$\eta_{t+1} = f(\eta_t, u_t, y_{ref,t}, d_t) + p_t \quad t = 1, 2, \dots, T \quad (2)$$

Model (2) captures all components of Figure 1 except for the yellow block. In operator form, (2) can be written as

$$\boldsymbol{\eta} = \mathbf{F}(\boldsymbol{\eta}, \mathbf{u}, \mathbf{y}_{ref}, \mathbf{d}) + \mathbf{p}, \quad (3)$$

where $\mathbf{F} : \ell^8 \times \ell^3 \times \ell^m \times \ell^3 \rightarrow \ell^8$ is a strictly causal operator.

A key assumption of the rPB framework is that the base system asymptotically tracks the references. This means that for all $\mathbf{d} \in \mathbf{D}$, $\mathbf{y}_{ref} \in \mathbf{Y}_{ref}$, $\mathbf{p} \in \ell_p$, and for $\mathbf{u} = 0$, the tracking error asymptotically goes to zero. In our case, the assumption is satisfied as the cascading PI architecture tracks the references under nominal conditions.

In (Kirsch et al., 2025), it is shown that if this condition is met, then under an Internal Model Control (IMC) architecture, all and only controllers capable to track the same references can be parametrized in terms of an operator \mathcal{M} generating ℓ_p signals when $\mathbf{p} \in \ell_p$. The IMC control architecture, which is shown in Figure 2, includes a copy of the system dynamics, which is used for computing the estimate $\hat{\mathbf{p}} = \boldsymbol{\eta} - \mathbf{F}(\boldsymbol{\eta}, \mathbf{u}, \mathbf{y}_{ref}, \mathbf{d})$ of the disturbance \mathbf{p} . In this setup, \mathbf{u} is chosen as:

$$\mathbf{u} = \mathcal{M}(\hat{\mathbf{p}}, \mathbf{y}_{ref}, \mathbf{d}), \quad (4)$$

for a causal operator $\mathcal{M} : \ell^8 \times \ell^3 \times \ell^3 \rightarrow \ell^m$. The intuition behind this control architecture is that given $\hat{\mathbf{p}} \in \ell_p$, the output of the rPB controller will also be an ℓ_p signal. It will thus decay to zero when the base system approaches steady state condition, thereby enabling the tracking of the reference.

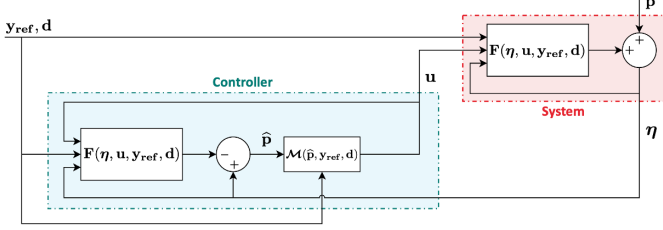


Fig. 2. IMC architecture parametrizing all reference tracking controllers in terms of one operator \mathcal{M}

The operator \mathcal{M} thus needs to generate ℓ_p sequences when $\hat{\mathbf{p}}$ is an ℓ_p signal, and irrespectively of \mathbf{y}_{ref} and \mathbf{d} which are not necessarily in ℓ_p . To this end, we factorize \mathcal{M} as follows:

$$\mathcal{M}(\hat{\mathbf{p}}, \mathbf{y}_{\text{ref}}, \mathbf{d}) = \mathcal{M}_2(\hat{\mathbf{p}}) * \mathcal{M}_\infty(\hat{\mathbf{p}}, \mathbf{y}_{\text{ref}}, \mathbf{d}), \quad (5)$$

with $\mathcal{M}_2 \in \mathcal{L}_p$ and $\mathcal{M}_\infty(\hat{\mathbf{p}}, \mathbf{y}_{\text{ref}}, \mathbf{d}) \in \ell_\infty$, $\forall \hat{\mathbf{p}} \in \ell_p, \mathbf{y}_{\text{ref}} \in \mathbf{Y}_{\text{ref}}$ and $\mathbf{d} \in \mathbf{D}$. The boundedness of \mathcal{M}_∞ ensures that $\mathcal{M}(\hat{\mathbf{p}}, \mathbf{y}_{\text{ref}}, \mathbf{d}) \in \ell_p$.

As shown in (Kirsch et al., 2025), searching over operators \mathcal{M} factorized as in (5) allows one to improve performance while preserving steady-state guarantees. However, optimizing directly over such \mathcal{M} constitutes an infinite-dimensional problem and is therefore intractable. To make the NOC formulation tractable, (Kirsch et al., 2025) proposes restricting the search for \mathcal{M}_2 to subsets of \mathcal{L}_2 that are described by a finite number of free parameters, while still being expressive enough to represent broad families of nonlinear controllers. This can be achieved using several operator models introduced in the literature, such as Recurrent Equilibrium Networks (Revay et al., 2024) or Structured State-Space Models (Gu et al., 2021; Massai and Ferrari-Trecate, 2025). In these frameworks, \mathcal{L}_2 operators are represented as parametrized dynamical systems interconnected with neural networks, enabling rich nonlinear behavior. The operator \mathcal{M}_∞ can then be parametrized as a Multilayer Perceptron (MLP) with a bounded output activation function, which also has a finite number of parameters.

By using the direct parametrization of (Revay et al., 2024, Section 5) for \mathcal{M}_2 and leveraging the naturally free parametrization of MLPs for \mathcal{M}_∞ , the rPB optimization problem becomes fully unconstrained. The parameters to optimize over become $\theta \in \mathbb{R}^d$, which includes the parameters of both \mathcal{M}_2 and \mathcal{M}_∞ .

We want to improve performance over a horizon T by solving a finite-horizon NOC, while also ensuring tracking is preserved even when the controller is applied for $t > T$. Considering an empirical average over a set of samples $\{(p_{T:0}^s, d_{T:0}^s)\}_{s=1}^S$ drawn from the distributions $\mathcal{P}_{T:0}$ and $\mathcal{D}_{T:0}$, this NOC problem can be expressed as:

Problem 1. Finite horizon unconstrained problem

$$\min_{\theta \in \mathbb{R}^d} \quad \frac{1}{S} \sum_{s=1}^S L(\eta_{T:0}^s, u_{T:0}^s, y_{ref,T:0}^s) \quad (6a)$$

$$\text{s. t. } \eta_t^s = f_t(\eta_t^s, u_t^s, y_{ref,t}^s, d_t^s) + w_t^s, \quad w_0^s = (x_0^s, v_0^s), \quad (6b)$$

$$u_t^s = \mathcal{M}_t(\theta)(w_{t:0}^s, y_{ref,t:0}^s, d_{t:0}^s), \quad \forall t = 0, 1, \dots, \quad (6c)$$

where $\eta_{T:0}^s$ and $u_{T:0}^s$ are the inputs and states obtained when the disturbances $p_{T:0}^s$ and $d_{T:0}^s$ are applied. As shown in (Kirsch et al., 2025), the absence of constraints on θ allows us to leverage powerful optimization frameworks such as PyTorch (Paszke, 2019), using a backpropagation-through-time approach (Werbos, 1990) to design the rPB controller efficiently.

The cost $L(\dots)$ in (6a) is completely free and can account for any behavior that is wished to be enforced. For the drive, as discussed in Section 4, the function L can be chosen for example to promote constraint satisfaction by using barrier functions. The rPB controller thus provides a way to improve the transient behavior of the system for any desired goal, without hindering the steady-state behavior induced by the base controller.

3.2 Input signal design

As described in the previous section, rPB can successfully preserve steady state guarantees because it outputs by construction ℓ_p signals when ℓ_p sequences are fed to \mathcal{M}_2 . However, this intrinsic property also implies that to successfully improve transient performance, the input signals to the rPB controller needs to be carefully designed. If not, the output of the rPB controller could be active when not needed, but more importantly it could already be decaying when it is required. The ideal signal would be non-zero during transient periods and immediately zero when the rPB controller is not needed anymore. Since δv_g is nonzero only during faults, these conditions are naturally satisfied by \mathbf{p} . Feeding its reconstruction $\hat{\mathbf{p}}$ to \mathcal{M}_2 excites the operator during the faults and not during nominal conditions.

Furthermore, by carefully selecting the signals fed to the operators \mathcal{M}_2 and \mathcal{M}_∞ , it is possible to embed contextual information into the rPB controller without altering its properties, thereby aiding the computation of effective control actions. As shown in (Kirsch et al., 2025), one way to do so is by passing these sequences only through \mathcal{M}_∞ . Here, we propose an alternative approach that allows these signals to also pass through \mathcal{M}_2 . To achieve this, we leverage the structure of \mathbf{p} . In particular, this sequence can be used to design a windowing signal that clamps all signals to zero under nominal conditions. Accordingly, we define the rectangular windowing signal $\sigma \in \ell^1$ as:

$$\sigma_t = \begin{cases} 1 & \text{if } \|p_t\| > \epsilon \\ 0 & \text{otherwise} \end{cases},$$

with $\epsilon \in \mathbb{R}$ a numerical tolerance. By using σ it is possible to window any signal $\mathbf{s} \in \ell^b$ as $s_{\sigma,t} = s_t * \sigma_t$. An intuitive way to understand is to see σ as a signal controlling a switching gate letting the other signals pass through to \mathcal{M}_2 or not. A block diagram of this setup can be found in Figure 3. By construction, \mathbf{s}_σ is an ℓ_p signal. Introducing

the windowing signal enables non- ℓ_p contextual information to be fed to \mathcal{M}_2 , improving its expressivity without compromising steady state guarantees. Incorporating this contextual information requires redefining \mathcal{M} by adding a fourth argument. The operator now maps $\mathcal{M} : \ell^8 \times \ell^3 \times \ell^3 \times \ell^c \rightarrow \ell^m$, where c specifies the dimension of the contextual information.

Remark 1. Passing the contextual information through \mathcal{M}_∞ ensures that it can influence the behavior of the rPB controller even when the switch in Figure 3 is open.

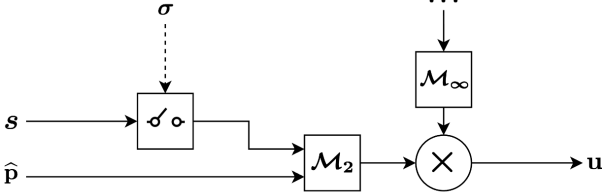


Fig. 3. Input signal structure to the operator \mathcal{M} . The switch logic is dictated by the condition on σ . The signals entering \mathcal{M}_∞ can be freely chosen.

Up to this point, we have only used the fault occurrence window for defining the time interval during which the rPB mechanism remains active. However, the transition back to nominal operating conditions also induces a short transient phase, during which keeping the rPB active may be beneficial. This allows for a smoother transition from the fault period with rPB to the steady-state under the base controller alone. Maintaining the switching signal active for a short, finite duration after the fault can therefore improve the post-fault response. Importantly, extending the rPB activity window by a finite amount does not compromise the ℓ_p nature of the outputs of \mathcal{M} , and the steady-state guarantees are preserved.

3.3 Interconnection with the base system

As mentioned in Section 3.1, the interconnection between the rPB output \mathbf{u} and the base system is unrestricted. In the base controller proposed in (Chandrasekaran et al., 2025), the modulation vector $m_{g,t}$ is saturated at each timestep to enforce input constraints. We choose to make \mathbf{u} act as an offset sequence to the modulation vector before saturation. The modulation vector is now computed as:

$$m_{g,t} = \text{sat}_{\|\cdot\| \leq \frac{1}{\sqrt{2}}} (m_{g,t}^b + u_t),$$

where $m_{g,t}^b$ is the modulation vector coming from the base controller and here $u_t \in \mathbb{R}^2$. We choose this interconnection because it is the place where the influence of the rPB can be the strongest, while still preserving input constraints thanks to the saturation.

By leveraging the windowing approach described in section 3.2, we have considerable freedom in choosing the signals that we feed to \mathcal{M}_2 . We choose \mathbf{s} such that for all t :

$$\mathbf{s}_t = [v_{dc,t}, i_{g,t}^\top, v_{g,t}^\top]^\top,$$

which is then windowed using σ to obtain \mathbf{s}_σ (see Figure 3). We also provide $\hat{\mathbf{p}}$ to \mathcal{M}_2 , but without windowing, as it is already an ℓ_2 signal. We choose to feed $\mathbf{s}_\infty = [\mathbf{d}^\top, \mathbf{p}^\top, v_{dc}, i_{g,t}^\top]^\top$ to \mathcal{M}_∞ , as it conveys valuable

information on the electrical state of the drive which is impacted by the faults. We thus get:

$$\mathbf{u} = \mathcal{M}_2(\mathbf{s}_\sigma, \hat{\mathbf{p}}) * \mathcal{M}_\infty(\mathbf{s}_\infty).$$

Furthermore, we feed these signals in per units. This serves as normalization, which facilitates the training for the neural network. Indeed, as the output of the rPB is directly saturated at $1/\sqrt{2}$, feeding it values orders of magnitude bigger than this bound would greatly hinder the learning.

4. SIMULATION RESULTS

This section describes the simulation results when applying the rPB approach to the drive for fault compensation. The main goal of the rPB controller is to preserve the DC bus voltage within a 2.5% range of its nominal voltage v_{dc}^{ref} , while also keeping the grid current under its maximum acceptable value. The loss function (6a) of the NOC problem is thus:

$$L(\eta_{T:0}, u_{T:0}, y_{ref,T:0}) = \sum_{t=0}^T \alpha_{nom} (v_{dc,t} - v_{dc}^{ref})^2 + \alpha_{r,v_{dc}} b(v_{dc,t}) + \alpha_{r,i_g} b(\|i_{g,t}\|),$$

where the terms α_{nom} , $\alpha_{r,v_{dc}}$, and α_{r,i_g} are scaling factors. The function $b : \mathbb{R} \rightarrow \mathbb{R}$ is a barrier function, which we choose as a squared ReLU:

$$b(x) = \text{ReLU}(x - x_{\max})^2 + \text{ReLU}(x_{\min} - x)^2,$$

where x_{\min} and x_{\max} are the bounds. We parametrize \mathcal{M}_2 as a REN with internal linear and nonlinear states of dimension twenty-two. For \mathcal{M}_∞ , we use a MLP consisting of four linear layers with widths 6, 10, 10, and 2, and apply sigmoid activations after each hidden layer.

4.1 Single phase drop

We consider nominal operation where the load on the mechanical side is $\tau_l = 0.95\tau_{max}$, where $\tau_{max} = 44.356kNm$ is the maximum torque the drive can supply. The drive operates at nearly full capacity. The setpoints to track are $v_{dc}^{ref} = 5000V$, $\omega^{ref} = 125.66rad/s$ and $Q^{ref} = 0VAR$. The constraints are $i_{g,max} = 2222A$ and $v_{dc} \in [0.975v_{dc}^{ref}, 1.025v_{dc}^{ref}]$.

We compare the response to a single phase loss fault with and without the rPB outer loop. We consider faults where the C phase of the grid voltage drops by a percentage value $\Delta \in \mathbb{R}$. Given the fault t_{start} and t_{end} times, the grid voltage in ABC coordinates is taken as:

$$\begin{aligned} v_{g,t}^A &= |V_g| \cos(2\pi ft) \\ v_{g,t}^B &= |V_g| \cos(2\pi ft - 2\pi/3) \\ v_{g,t}^C &= \begin{cases} (1 - \Delta)|V_g| \cos(2\pi ft + 2\pi/3) & \text{if } t \in [t_{start}, t_{end}] \\ |V_g| \cos(2\pi ft + 2\pi/3) & \text{otherwise} \end{cases} \end{aligned}$$

where $|V_g| = 3150V$ is the nominal grid voltage norm and $f = 50Hz$ is the grid frequency.

To train the rPB controller, we generate a dataset of v_g sequences containing drops of phase C of around 300ms, and converted to $\alpha\beta$ coordinates. We slightly change the length of the fault between different profiles to cover endings occurring over the entire oscillation period of the

grid voltage. The profiles also differs in the scale of the drop, with Δ sampled from a uniform distribution between 0 and 1. The generated dataset is composed of 300 samples.

As outlined in Section 3.2, σ is held at 1 briefly after the fault is cleared. In this implementation, the switch remains closed until the next zero crossing of $v_{g,\beta}$. Enforcing the switching instant at a zero crossing results in a smoother transition, since the β -component coincides with its fault-free value at that point.

We train the rPB controller using stochastic gradient descent with Adam for 2600 epochs, setting a learning rate of 1×10^{-3} .

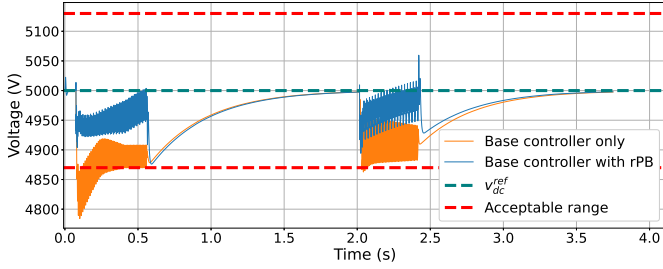


Fig. 4. Evolution of the DC bus voltage with and without the trained rPB controller

The v_{dc} profiles with and without the rPB controller are shown in Figure 4 for a test profile (not seen during control design) with two faults: the first one is a full drop of phase ($\Delta = 1$) lasting for about 600ms and the second one is a 60% drop lasting for around 400ms. Both event end at different times within the grid voltage period. Without rPB, the AFE controller struggles to keep the DC bus voltage within bounds, reaching a minimum below 4800 V, whereas with rPB the lower bound is never violated. Furthermore, the base controller induces constraints violations for more than 300ms during the first fault, which would be enough time to trigger a drive shutdown. By allowing the system to stay within safe regions the rPB allows the continuation of operation even during faults, significantly improving the performance of the drive. During the second fault, the base controller mostly keeps the DC bus voltage within the bounds but strongly reduces it while the rPB controller keeps the DC bus voltage closer to its nominal value, reducing the strain on the drive, and showing that the neural network generalizes well to several depths of drops. Looking at the periods in between faults, we can see that the trajectories with and without rPB converge to the same trajectory tracking the nominal value, showcasing how the rPB controller does not hinder steady state properties.

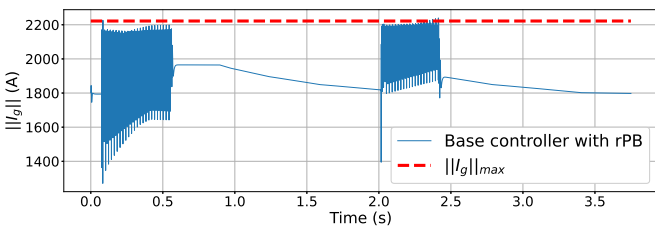


Fig. 5. Evolution of the grid current norm with the trained rPB controller

Although the main objective for the rPB controller in this experiment is to keep the DC bus in safe operating conditions, it is important to see if it does so at the expense of the other states of the drive. Currently, rPB has no influence on the mechanical quantities of the drive as τ_m is not modified by it. rPB therefore cannot have a negative impact on the angular speed. For the grid side, Figure 5 shows the evolution of the grid current norm under the rPB outer loop. The neural network controller effectively learns to keep the current norm below its prescribed upper bound. Only brief, minor peaks slightly exceed the limit, and the rPB does not cause any sustained constraint violations. Such short-lived violations are acceptable for drive operation and are too small to pose any risk to the system. Overall, the rPB controller improves the DC bus voltage regulation during faults without compromising the safety of the other drive states.

Both with and without rPB, the faults induce oscillations in the DC bus voltage and in the grid current. It is therefore worth analyzing the spectra for both control strategies to assess whether some problematic harmonics have been generated, especially for the grid current. The spectra of the α and β coordinates of the grid current during the first fault are shown in Figure 6.

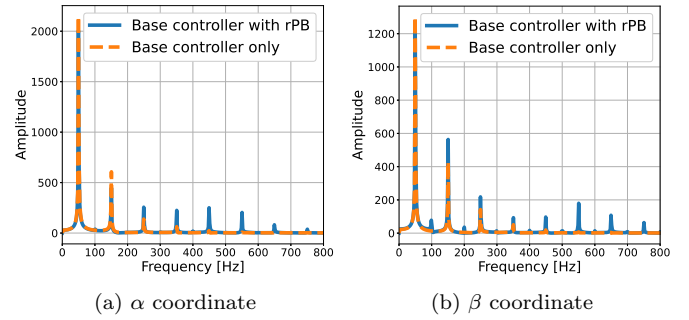


Fig. 6. Frequency spectra of the α and β coordinates of the grid current with and without the rPB controller.

The main peak in both the α and β spectra occurs at 50 Hz under both control schemes, corresponding to the grid's fundamental frequency. The most significant harmonics appear at 150 Hz and 250 Hz due to the single-phase loss, which is typical for such grid faults. Both approaches exhibit similar magnitudes at these lower-order harmonics, indicating that the fundamental and main harmonic content is predominantly governed by the fault and not drastically altered by the rPB addition. For higher frequencies the controller with rPB introduces relatively smaller harmonics, which are most pronounced around 550 Hz and 650 Hz in the β coordinate. These additional peaks remain significantly lower in amplitude than the one at 50 Hz. The emergence of these higher-order harmonics in the presence of rPB can be attributed to the rPB controller's dynamics in response to unbalanced fault conditions. Nevertheless, their limited amplitude suggests that the influence of rPB is not a concern for the grid.

Another relevant aspect to examine is how the rPB outer loop alters the modulation vector m_g . Figure 7 shows the norm of the modulation vector around the beginning of the first fault. In both the baseline and rPB-modified cases, the signal is periodic during the fault. However, the profile

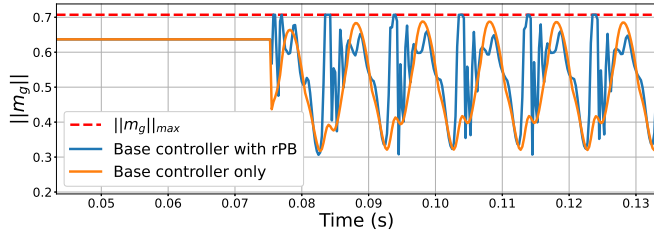


Fig. 7. Evolution of the modulation vector norm with and without rPB at the end of the fault.

resulting from the rPB controller exhibits a less regular intra-period structure. The overall norm is greater when utilizing rPB, which underscores its role in increasing the effective control strength. Focusing on the onset of the fault, the rPB strategy induces two distinct peaks where the modulation norm reaches its maximum permissible value, whereas the baseline controller's norm decreases over this interval. These peaks increase the instantaneous modulation amplitude and therefore allow the DC bus to draw more power from the grid during the fault, helping the DC bus to compensate the initial strong voltage drop. Because the rPB offset is introduced prior to actuator saturation, the input constraints remain satisfied over the whole trajectory.

In the interest of space, we have limited the results presented here to the electrical states of the drive, where the rPB has the most pronounced impact. More comprehensive simulation results are provided in Appendix A.

5. CONCLUSION

The rPB framework has been successfully integrated into a medium voltage drive system with an active front-end, ensuring safe and continuous operation during various grid fault scenarios. By designing input signals that leverage the grid voltage norm, rPB activation is precisely timed to coincide with the presence and duration of faults, independent of their recurrence or length. Our results with single-phase faults demonstrate that rPB reduces the DC bus voltage drop, supporting safe drive operation, and keeps the grid current within permissible limits. In the event of a phase loss near full load, the rPB controller prevents violations severe enough to otherwise trigger a system shutdown. These benefits underline the strong operational resilience provided by rPB. Future research should explore extending rPB's effect to the mechanical side of the drive, by enabling it to actuate the motor torque. Another promising direction is to make the rPB able to address all classes of grid faults. Currently, rPB is tailored for a specific case, but incorporating more contextual inputs could enable fault-type-agnostic compensation. A possible way to do so would be to feed the prediction of a dynamic fault classifier to the rPB controller.

REFERENCES

Arghir, C., Jörg, P., and Mastellone, S. (2025). Transferring the driveshaft inertia to the grid via the dc-link in mv drive systems. *arXiv preprint arXiv:2508.21760*.

Baeckeland, N., Chatterjee, D., Lu, M., Johnson, B., and Seo, G.S. (2024). Overcurrent limiting in grid-forming inverters: A comprehensive review and discus-

sion. *IEEE Transactions on Power Electronics*, 39(11), 14493–14517. doi:10.1109/TPEL.2024.3430316.

Bottrell, N. and Green, T.C. (2014). Comparison of current-limiting strategies during fault ride-through of inverters to prevent latch-up and wind-up. *IEEE Transactions on Power Electronics*, 29(7), 3786–3797. doi:10.1109/TPEL.2013.2279162.

Chandrasekaran, S., Arghir, C., Joerg, P., Doerfler, F., and Mastellone, S. (2025). Reactive power flow optimization in ac drive systems. URL <https://arxiv.org/abs/2504.10360>.

Eslahi, M.S., Vaez-Zadeh, S., and Rodriguez, J. (2023). Resiliency enhancement and power quality optimization of converter-based renewable energy microgrids. *IEEE Transactions on Power Electronics*, 38(6), 7785–7795.

Ferramosca, A., Limon, D., Alvarado, I., Alamo, T., and Camacho, E. (2009). Mpc for tracking of constrained nonlinear systems. In *Proceedings of the 48th IEEE Conference on Decision and Control (CDC) held jointly with 2009 28th Chinese Control Conference*, 7978–7983. doi:10.1109/CDC.2009.5400618.

Gao, C., Yan, J., Zhou, S., Varshney, P.K., and Liu, H. (2019). Long short-term memory-based deep recurrent neural networks for target tracking. *Information Sciences*, 502, 279–296.

Geyer, T., Papafotiou, G., and Morari, M. (2008). Model predictive direct torque control—part i: Concept, algorithm, and analysis. *IEEE Transactions on Industrial Electronics*, 56(6), 1894–1905.

Gu, A., Goel, K., and Ré, C. (2021). Efficiently modeling long sequences with structured state spaces. *arXiv preprint arXiv:2111.00396*.

He, X., Desai, M.A., Huang, L., and Dörfler, F. (2024). Cross-forming control and fault current limiting for grid-forming inverters. *IEEE Transactions on Power Electronics*.

Hokayem, P., Jörg, P., Mastellone, S., and Schweizer, M. (2024). Control of electric power conversion systems. *The Impact of Automatic Control Research on Industrial Innovation: Enabling a Sustainable Future*, 135–167.

Hossein-zadehtaher, M., Zare, A., Khan, A., Umar, M.F., D'silva, S., and Shadmand, M.B. (2024). Ai-based technique to enhance transient response and resiliency of power electronic dominated grids via grid-following inverters. *IEEE Transactions on Industrial Electronics*, 71(3), 2614–2625. doi:10.1109/TIE.2023.3265067.

Kirsch, N., Massai, L., and Ferrari-Trecate, G. (2025). Boosting the transient performance of reference tracking controllers with neural networks. URL <https://arxiv.org/abs/2504.00845>.

Kong, L., He, W., Liu, Z., Yu, X., and Silvestre, C. (2023). Adaptive tracking control with global performance for output-constrained mimo nonlinear systems. *IEEE Transactions on Automatic Control*, 68(6), 3760–3767. doi:10.1109/TAC.2022.3201258.

Limon, D., Ferramosca, A., Alvarado, I., and Alamo, T. (2018). Nonlinear mpc for tracking piece-wise constant reference signals. *IEEE Transactions on Automatic Control*, 63(11), 3735–3750. doi:10.1109/TAC.2018.2798803.

Massai, L. and Ferrari-Trecate, G. (2025). Free parametrization of l2-bounded state space models. *arXiv preprint arXiv:2503.23818*.

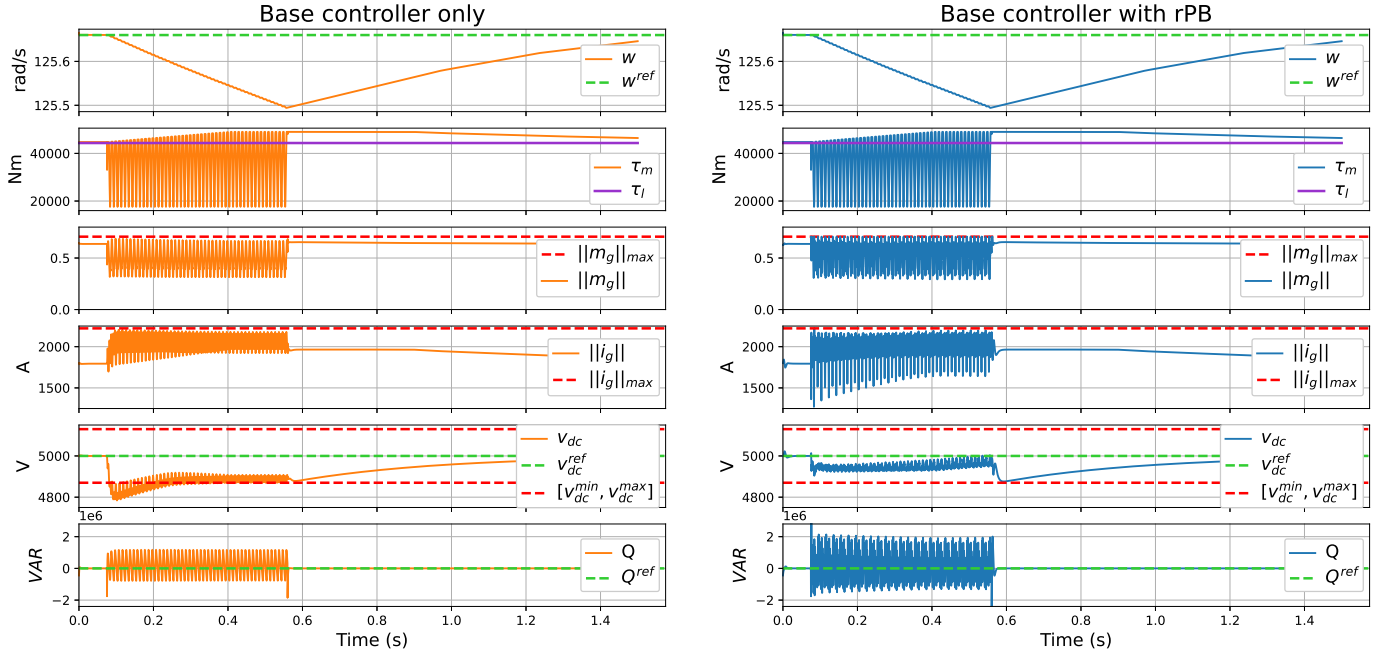


Fig. 8. The first two rows show the behaviour of the mechanical variables. The third row illustrates the evolution of the modulation vector, and the last three rows present the electrical quantities.

- Nguyen, N.T. (2018). *Model-Reference Adaptive Control*, 83–123. Springer International Publishing, Cham. doi:10.1007/978-3-319-56393-0_5.
- Park, B.S., Kwon, J.W., and Kim, H. (2017). Neural network-based output feedback control for reference tracking of underactuated surface vessels. *Automatica*, 77, 353–359. doi:https://doi.org/10.1016/j.automatica.2016.11.024.
- Paszke, A. (2019). Pytorch: An imperative style, high-performance deep learning library. *arXiv preprint arXiv:1912.01703*.
- Rawlings, J.B., Mayne, D.Q., Diehl, M., et al. (2017). *Model predictive control: theory, computation, and design*, volume 2. Nob Hill Publishing Madison, WI.
- Revay, M., Wang, R., and Manchester, I.R. (2024). Recurrent equilibrium networks: Flexible dynamic models with guaranteed stability and robustness. *IEEE Transactions on Automatic Control*, 69(5), 2855–2870. doi:10.1109/TAC.2023.3294101.
- Schneeberger, M., Dörfler, F., and Mastellone, S. (2024). Advanced safety filter for smooth transient operation of a battery energy storage system. In *2024 IEEE 63rd Conference on Decision and Control (CDC)*, 2385–2390. IEEE.
- Stanojev, O., Karaca, O., and Schweizer, M. (2025). Grid-forming vector current control frt modes under symmetrical and asymmetrical faults. *Sustainable Energy, Grids and Networks*, 101830.
- Tang, Y., Luo, G., and Pu, Y. (2025). Short-circuit calculation approach of grids with high proportion of inverter-interfaced generator stations. *Electric Power Systems Research*, 241, 111407. doi:https://doi.org/10.1016/j.epsr.2024.111407.
- Tiitinen, P. and Surandra, M. (1996). The next generation motor control method, dte direct torque control. In *Proceedings of International Conference on Power Electronics, Drives and Energy Systems for Industrial Growth*, volume 1, 37–43. IEEE.
- Wang, H., Watson, J.D., and Watson, N.R. (2025). An improved control strategy for gfm-based control of type-iv wind turbine under normal and grid fault conditions. *IEEE Transactions on Power Delivery*, 1–11. doi:10.1109/TPWRD.2025.3606626.
- Werbos, P.J. (1990). Backpropagation through time: what it does and how to do it. *Proceedings of the IEEE*, 78(10), 1550–1560.
- Zarei, S.F., Mokhtari, H., Ghasemi, M.A., and Blaabjerg, F. (2019). Reinforcing fault ride through capability of grid forming voltage source converters using an enhanced voltage control scheme. *IEEE Transactions on Power Delivery*, 34(5), 1827–1842. doi:10.1109/TPWRD.2018.2844082.
- Zhang, J.X., Yang, T., and Chai, T. (2022). Neural network control of underactuated surface vehicles with prescribed trajectory tracking performance. *IEEE Transactions on Neural Networks and Learning Systems*.

Appendix A. COMPLEMENTARY RESULTS

We present in here the complementary results to the ones presented in the main paper. The evolution of the key drive parameters for the first 1.5 seconds are plotted in Figure 8. This interval contains the full loss of phase fault and the recovery towards nominal conditions. During the fault, we can see that the angular speed of the shaft decreases. This is because the drop in supplied grid voltage limits the maximum active power which can be delivered to the shaft and thus the torque. The available torque thus become insufficient to compensate the load, reducing the angular speed. Still, the scale of the drop is negligible, reaching at most 0.1% of the nominal angular speed. An important observation is that the angular velocity and the torque profiles are the same with and without rPB, which makes sense as it only influences the modulation vector m_g .